Predicting the Three-Dimensional Structure of Human P-Glycoprotein in Absence of ATP by Computational Techniques Embodying Crosslinking Data: Insight into the Mechanism of Ligand Migration and Binding Sites

Stéphane Vandevuer,[1] Françoise Van Bambeke,[2] Paul M. Tulkens,[2] and Martine Prévost[1]*
[1]*Bioinformatique génomique et structurale, Université Libre de Bruxelles, Bruxelles, Belgium*
[2]*Unité de Pharmacologie cellulaire et moléculaire, Université catholique de Louvain, Bruxelles, Belgium*

ABSTRACT P-glycoprotein is a membrane protein involved in the phenomenon of multidrug resistance. Its activity and transport function have been largely characterized by various biochemical studies and a low-resolution image has been obtained by electron microscopy. Obtaining a high-resolution structure is, however, still remote due to the inherent difficulties in the experimental determination of membrane protein structures. We present here a three-dimensional (3D) atomic model of P-glycoprotein in absence of ATP. This model was obtained using a combination of computational techniques including comparative modeling and rigid body dynamics simulations that embody all available cysteine disulfide crosslinking data characterizing the whole protein in absence of ATP. The model features rather well most of the experimental interresidue distances derived both in the transmembrane domains and in the nucleotide binding domains. The model is also in good agreement with electron microscopy data, particularly in terms of size and topology. It features a large cavity detected in the protein core into which seven ligands were successfully docked. Their predicted affinity correlates well with experimental values. Locations of docked ligands compare favorably with those suggested by cysteine-scanning data. The finding of different positions both for a single ligand and for different ligands corroborates the experimental evidence indicating the existence of multiple drug binding sites. The interactions identified between P-glycoprotein and the docked ligands reveal that different types of interactions such as H-bonds, π–π and cation–π interactions occur in agreement with a recently proposed pharmacophore model of P-glycoprotein ligands. Furthermore, the model also displays a lateral opening located in the transmembrane domains connecting the lipid bilayer to the central cavity. This feature supports rather well the commonly admitted mechanism of substrate uptake from the lipid bilayer. We propose that this 3D model may be an important tool to understand the structure–function relationship of P-glycoprotein. Proteins 2006;63:466–478. © 2006 Wiley-Liss, Inc.

INTRODUCTION

The P-glycoprotein (P-gp), product of the *mdr1* gene in humans, is an ATP-dependent transporter that extrudes a large range of structurally diverse compounds out of eucaryotic cells. P-gp is found at the level of elimination organs, like intestines, kidney, and liver, where it is involved in the secretion of drugs and metabolites, as well as at the blood–brain barrier, where its efflux activity prevents the accumulation of cytotoxic agents in the central nervous system.[1,2] The overexpression of P-gp is also associated with a multidrug resistance phenotype in various forms of cancer,[3] causing suboptimal outcomes in chemotherapy.

P-gp is a member of the ATP-binding cassette (ABC) family of transporters.[4,5] It is a single polypeptide of 1280 residues, organized as two homologous halves (which are 43% identical in human P-gp) of ~ 610 residues joined by a ~ 60 residues linker. Each half consists of six transmembrane (TM) segments followed by a cytoplasmic nucleotide-binding domain (NBD). The two halves of P-gp are essential for the activity of the transporter. They cannot act autonomously and instead appear to function coordinately, suggesting that they interact in some fashion. Several helices of the TM domains have been proposed to

---

contain the binding site(s) and consequently are believed to form the pathway through which the substrates cross the membrane. On the other hand, the NBDs couple the energy associated with ATP binding and hydrolysis to drug transport.[6] The linker of ~ 60 residues does not appear to be essential to the protein function though when present its flexibility appears to be a prerequisite.[7]

The P-gp mediated-transport mechanism has been extensively studied but remains controversial. Briefly, it is believed[8,9] that the transport cycle is initiated by substrate binding in the TM domains of P-gp, which increases the ATP affinity for the protein. After binding and/or hydrolysis of a first ATP molecule in one of the NBDs several restructurings occur in the TM domains of the protein. This conformational change allows the release of the drug to the extracellular medium. After hydrolysis of a second ATP molecule P-gp returns to its original configuration. The protein is then reset for another cycle.

A first low-resolution structure obtained by electron microscopy (EM) on detergent solubilized P-gp suggests that the TM domains form a cone-shaped chamber in the membrane, open towards the extracellular face.[10] A second structure was obtained by EM for the protein reconstituted in a lipid bilayer.[11] This structure, which is the only one representative of the protein in its native environment, presents P-gp in a conformation in which the two NBDs are in close interaction. A third structure, derived at a resolution of 8 Å for P-gp bound to a nonhydrolysable analog of ATP,[12] provides valuable data on the spatial arrangement of the TM helices and the NBDs. Mutagenesis,[13] photoaffinity labeling,[14] and cysteine scanning and crosslinking studies[15–25] have identified several residues involved in drug binding in the TM domains and have permitted to obtain structural information on the interactions between the TM domains and between the NBDs. These studies, however, do not supply with a detailed atomic structure of P-gp, which would be of considerable help in elucidating the molecular mechanism for substrate binding and release.

Crystallization of membrane proteins to obtain direct information on three-dimensional (3D) structure is still a difficult task. At this time three different 3D models of P-gp at an atomic level have been elaborated,[26–28] but none of them fully takes into account the available experimental structural data. We therefore present here a new 3D model that was elaborated by the combination of different computational methods such as comparative modeling and rigid body dynamics. We used the structure of *E. coli* MsbA[29] as a template to generate an initial model. However, we did not exploit the structure of the dimer as its structural features do not match those expected for P-gp structure. Instead we resorted to the structure of each monomer independently to model the two halves of P-gp. To feature the close association of the two NBDs in P-gp as witnessed by several experimental studies, the 3D structure of BtuCD[30] was also used. Rigid body dynamics involving distance-restrained potentials was then applied to the initial model. This step was performed to include in our model cysteine-scanning mutagenesis

data describing helices orientation and interresidue distances. The validity of the model is then discussed in regard to the available experimental data.

The interaction of compounds with P-gp is clearly a complex process. A general pharmacophore model of P-gp drugs has been recently proposed,[31] and involves two hydrophobic points, three H-bond acceptor points and one H-bond donor point organized in a precise geometry. Our 3D model was therefore used to dock several ligands in the central cavity harbored by the TM domains. The geometry of interaction of the ligands and their predicted affinity are examined and compared with the experimental data.

MATERIALS AND METHODS
Sequences Alignment

All protein sequences were obtained from the Swiss-Prot data base. The sequences of the N- and C-terminal halves of P-gp (residues 1–630 and 690–1280, respectively) were aligned pairwise with the sequence of *E. coli* MsbA monomer using the program ClustalW.[32]

The sequences of the NBD of each P-gp half (residues 386–630 and 1029–1280) were aligned with NBDs of closely related ABC transporters (*E. coli* BtuCD, *E. coli* MsbA, *P. fur.* Rad50, and MJ0796) using ClustalW.

The alignment of the sequences used in the comparative modeling process is shown in Figure 1.

Comparative Modeling

E. coli MsbA is the protein with the highest percentage of sequence identity to P-gp whose 3D structure is known. However, for reasons explained in the Results and Discussion section, we did not use the dimeric structure because of its complete discrepancy with the experimental data on P-gp. Nevertheless we resorted to each MsbA monomer as a template to generate an initial model of each P-gp half using the sequence alignment shown in Figure 1.

The X-ray structure of MsbA[29] (PDB code: 1JSQ) contains the Cα atom positions only. The structure of *E. coli* MsbA was then completed by using MaxSprout,[33] a database algorithm to generate the missing protein backbone and sidechains. Additional templates for P-gp modeling were searched with the Blast program[34] for the tiny portions for which there is no corresponding 3D structure in MsbA (see Fig. 1). Three structures were found (PDB codes: 1F3M, 1JJ7, 1FB3).

Modeling of the P-gp NBD dimer was performed using as templates the NBD dimer of BtuCD and each NBD monomer of MsbA following the alignment given in Figure 1. The BtuCD structure[30] (PDB code: 1L7V) is a good template to model the close association of the dimeric structure of the NBDs and the relative orientation of each P-gp monomer, as observed experimentally.

Comparative modeling was performed with the Modeller 5 software,[35] using the model routine with the alignments described on Figure 1. Ten models were generated, and the structure with the most favorable intramolecular energy, as described by the objective function of the program, was selected to represent an initial model.

```
P-gp   112  TRYAYYYSGIGAGVLVAAYIQVSFWCLAAGRQIHKIRKQFFHAIMRQEIGWFDVHDVGELNTRLTDDVSKINEGIGDKIGMFFQSMATFFTGFIVGFTRG   211
MsbA    65  VWMPLVVIGLMILRGITSYVSSYCISWVSGKVVMTMRRRLFGHMMGMPVSFFDKQSTGTLLSRITYDSEQVASSSSGALITVVREGASIIGLFIMMFYYS   164
BtuD        ---------------------------------------------------------------------------------------------------
1F3M        ---------------------------------------------------------------------------------------------------
1JJ7        ---------------------------------------------------------------------------------------------------

P-gp   212  WKLTLVILAISPVLGLSAAVWAKILSSFTDKELLAYAKAGAVAEEVLAAIRTVIAFGGQKKELERYNKNLEEAKRIGIKKAITANISIGAAFLLIYASYA   311
MsbA   165  WQLSIILIVLAPIVSIAIRVVSKRFRNISKNMQNTMGQVTTSA---------------------------RLQGMKMVSASSISDPIIQLIASLALA      264
BtuD        ---------------------------------------------------------------------------------------------------
1F3M    C1  -----------------------------------------SDEEILEKLRSIVSVGDPKKKYTRFEKIGQGASG-------------------------   C34
1JJ7        ---------------------------------------------------------------------------------------------------

P-gp   312  LAFWYGTTLVLSGEYSIGQVLTVFFSVLIGAFSVGQASPSIEAFANARGAAYEIFKIIDNKPSIDSYSKSGHKPDNIKGNLEFRNVHFSYPSRKEVKILK   411
MsbA   265  FVLYAASFPSVMDSLTAGTITVVFSSMIALMRPLKSLTNVNAQFQRGMAACQTLFTILDSEQEKD---EGKRVIERATGDVE-----------------   343
BtuD     2  ----------------------------------------------------------------SIVMQLQDVA-------ESTRLG             17
1F3M        ---------------------------------------------------------------------------------------------------
1JJ7   A14  -------------------------------------------------------------VQFQDVSFAYPNRPDVLVLQ                    A34

P-gp   412  GLNLKVQSGQTVALVGNSGCGKSTTVQLMQRLYDPTEGMVSVDGQDIRTINVRFLREIIGVVSQEPVL-FATTIAENIRYGR-ENVTMDEIEKAVKEANA   509
MsbA   419  ---------------------------------------------------VALVSQNVHL-FNDTVANNIAYARTEQYSREQIEEAARMAYA         459
BtuD    18  PLSGEVRAGEILHLVGPNGAGKSTLLARMAGMTSGK-GSIQFAGQPLEAWSATKLALHRAYLSQQQTPPFATPVWHYLTLHQ-HDKTRTELLNDVAGALA   115
1F3M        --------------------------------------------------------------------------------------------
1JJ7   A35  GLTFTLRPGEVTALVGPNGSGKSTVAALLQNLYQPTGGQLLLDGKPLPQYEHRYLHRQVA----------------------------------        A94

P-gp   510  YDFIMKLPHKFDTLVGERGAQLSGGQKQRIAIARALVR-----NP--KILLLDEATSALDTESEAVVQVALDKA--RKGRTTIVIAHRLS-TVRNADVIA   599
MsbA   460  MDFINKMDNGLDTVIGENGVLLSGGQRQRIAIARALLR-----DS--PILILDEATSALDTESERAIQAALDEL--QKNRTSLVIAHRLS-TIEKADEIV   549
BtuD   116  ----------LDDKLGRSTNQLSGGEWQRVRLAAVVLQITPQANPAGQLLLLDEPMNSLDVAQQSALDKILSALCQ-QGLAIVMSSHDLNHTLRHAHRAW   204
1F3M        ---------------------------------------------------------------------------------------------------
1JJ7        ---------------------------------------------------------------------------------------------------

P-gp   510  GFDDGVIVEKGNHDE     614
MsbA   550  VVEDGVIVERGTHND     564
BtuD   205  LLKGGKMLASGRREE     219
1F3M        ---------------
1JJ7        ---------------
```

```
P-gp   753  NLFSLLFLALGIISFITFFLQGFTFGKAGEILTKRLRYMVFRSMLRQDVSWFDDPKNTTGALTTRLANDAAQVKGAIGSRLAVITQNIANLGTGIIISFI   852
MsbA    65  VWMPLVVIGLMILRGITSYVSSYCISWVSGKVVMTMRRRLFGHMMGMPVSFFD--KQSTGTLLSRITYDSEQVASSSSGALITVVREGASIIGLFIMMFY   162
BtuD        ---------------------------------------------------------------------------------------------------
1FB3        ---------------------------------------------------------------------------------------------------
1JJ7        ---------------------------------------------------------------------------------------------------

P-gp   853  YGWQLTLLLLAIVPIIAIAGVVEMKMLSGQALKDKKELEGAGKIATEAIENFRTVVSLTQEQ---KFEHMYAQSLQVPYRNSLRKAHIFGITFSFTQAMM   949
MsbA   163  YSWQLSIILIVLAPIVSIAIRVVSKRFRNISKNMQNTMGQVTTSA--------------------------RLQGMKMVSASSISDPIIQLIA         259
BtuD        ---------------------------------------------------------------------------------------------------
1FB3  A201  ------------------------------------------MKEKAPENFRLDFAVSREQTNEKGEKMYIQTRMAQYA-------------------   A237
1JJ7        ---------------------------------------------------------------------------------------------------

P-gp   950  YFSYAGCFRFGAYLVAHKLMSFEDVLLVFSAVVFGAMAVGQVSSFAPDYAKAKISAAHIIMIIEKTPLIDSYSTEGLMPNTLEGNVTFGEVVFNYPTRPD   1049
MsbA   260  SLALAFVLYAASFPSVMDSLTAGTITVVFSSMIALMRPLKSLTNVNAQFQRGMAACQTLFTILDSEQEKD---EGKRVIERATGDVE-------------   343
BtuD     2  ----------------------------------------------------------------SIVMQLQDVA-------E                   12
1FB3        ---------------------------------------------------------------------------------------------------
1JJ7   A15  ------------------------------------------------------------VQFQDVSFAYPNRPD                          A29

P-gp  1050  IPVLQGLSLEVKKGQTLALVGSSGCGKSTVVQLLERFYDPLAGKVLLDGKEIKRLNVQWLRAHLGIVSQEPIL-FDCSIAENIAYGDNSRVVSQEEIVRA   1148
MsbA   419  -----------------------------------------------VALVSQNVHL-FNDTVANNIAYARTEQ-YSREQIEEA                  453
BtuD    13  STRLGPLSGEVRAGEILHLVGPNGAGKSTLLARMAGMTSGK-GSIQFAGQPLEAWSATKLALHRAYLSQQQTPPFATPVWHYLTLHQHD--KTRTELLND   109
1FB3        ---------------------------------------------------------------------------------------------------
1JJ7   A30  VLVLQGLTFTLRPGEVTALVGPNGSGKSTVAALLQNLYQPTGGQLLLDGKPLPQYEHRYLHRQVA----------------------------------   A94

P-gp  1149  AKEANIHAFIESLPNKYSTKVGDKGTQLSGGQKQRIAIARALVR-------QPHILLLDEATSALDTESEKVVQEALDKA--REGRTCIVIAHRLS-TIQ   1238
MsbA   454  ARMAYAMDFINKMDNGLDTVIGENGVLLSGGQRQRIAIARALLR-------DSPILILDEATSALDTESERAIQAALDEL--QKNRTSLVIAHRLS-TIE   543
BtuD   110  V--AGAL--------ALDDKLGRSTNQLSGGEWQRVRLAAVVLQITPQANPAGQLLLLDEPMNSLDVAQQSALDKILSALCQ-QGLAIVMSSHDLNHTLR   198
1FB3        ---------------------------------------------------------------------------------------------------
1JJ7        ---------------------------------------------------------------------------------------------------

P-gp  1239  NADLIVVFQNGRVKEHGTHQQ    1259
MsbA   544  KADEIVVVEDGVIVERGTHND    564
BtuD   199  HAHRAWLLKGGKMLASGRREE    219
1FB3        --------------------
1JJ7        --------------------
```

Fig. 1. Alignment of the sequences used in the comparative modeling procedure. (Top panel) Alignment to the N-terminal half of P-gp. (Bottom panel) Alignment to the C-terminal half of P-gp. The first line is the P-gp sequence to be modeled; second line is the sequence of MsbA; third line is the sequence of BtuCD (used for the modeling of the NBDs); and the last two lines are sequences of protein structures used to model tiny portions of P-gp for which stucture is missing in MsbA.

The initial model of each P-gp half was then fitted on the NBD dimer model. The fitting was performed using the positions of the C_α atoms.

Rigid Body Molecular Dynamics

Starting from the model issued from the comparative modeling and fitting procedure, a P-gp 3D model was

generated by resorting to multibody molecular dynamics simulations. This approach is a multigranular modeling whereby different parts of the molecule are modeled at different levels of detail.[36] The molecular system is sub-structured in rigid bodies and atomistic-described regions. The molecular dynamics simulation was performed with the CHARMM c27b3 software.[37] The transmembrane helices and the NBDs were substructured as separate rigid bodies. These bodies are allowed to undergo large motions relative to each other but no motion occurs within a body. The remaining loops connecting helices and NBDs were treated as atomic particles or single atom bodies.

For the modeling of the partial model (i.e., helices 4, 5, 6, 10, 11, 12, NBD1, and NBD2), three successive molecular dynamics simulations of 30,000 steps were performed. For the modeling of the final model (adding helices 2, 3, 8, and 9 to the previous model), a single molecular dynamics simulation of 30,000 steps was performed. All the simulations were performed using the Lobatto integrator with a time step of 1 fs. The temperature of the bath was set to 50 K in order to avoid excessive heating of the system.

Force-field interactions were obtained by a conventional all-atom CHARMM force field (CHARMM22).[38] Distance-based restraint potentials were added to the classical potentials so as to account for structural experimental evidence. These distances were derived from cysteine crosslinking experiments with two types of reactants.[15,16,18–21,27] When crosslinking between two residues was observed with $Cu^{2+}(phen)_3$ as oxydant at a temperature of 4°C, a distance of 8 to 10 Å between the two $C\alpha$ atoms involved was used. For the experiments performed at 21°C or 37°C, the maximum distance value was increased to 15 Å in order to take into account the increased mobility of the protein. When crosslinking was observed with methanethiosulfonate (MTS) compounds as substrates, a 3D model of their structure was generated using the Corina program.[39] The distances were then derived by measuring the end-to-end distance of the 3D structure of these molecules. The distances measured this way may somewhat differ from those given in the papers of Loo and Clark.[15,16,18–21] Table I lists the distance values assigned in the rigid body dynamics procedure.

Each rigid body molecular dynamics was followed by an energy minimization of 500 steps with the steepest descent algorithm.

In order to proceed with the docking experiments positioning of the sidechains was performed again with the specialized program SCWRL.[40]

Docking

In order to assign the correct protonation state of each molecule, pKa values were obtained either from experimental data or predicted using the ChemSilico program.[41] According to these values all the ligands bear a positive charge at physiological pH. Verapamil was built as R-verapamil (also known as dexverapamil). It is indeed known that racemic verapamil and R-verapamil have identical inhibition constant values.[42] The 3D structures of the ligands were generated with the Corina program.

Their atomic partial charges were computed with MOPAC using the semiempirical MNDO Hamiltonian.[43] The atomic partial charges for the protein were taken from the CHARMM19 force field.[37]

Docking was performed with the Autodock program (v. 3.0),[44] using the implemented genetic algorithm and the default parameters. Twenty-five independent docking runs were performed for each ligand.

RESULTS AND DISCUSSION
Modeling of P-gp Structure

Because the structure of P-gp undergoes several conformational changes along its catalytic cycle, it is important to decide which conformation to model, and carefully sort the experimental data describing it. We chose to produce a model reflecting the structure of P-gp in absence of ATP. This structure has been extensively studied by cysteine scanning mutagenesis and cysteine disulfide crosslinking experiments,[15–25] which permitted to obtain important structural information about the relative positions of different parts of the TM domains, NBDs, and on the substrate binding site(s).

The search for proteins of known structure which share at least 20% of global sequence identity with P-gp, produced only two possibilities: the structures of MsbA of *E. coli*[29] (PDB code: 1JSQ) and of *V. cholera*[45] (PDB code: 1PF4). Both structures were recently determined by X-ray spectroscopy to a 4.5 and 3.8 Å resolution, respectively. The two proteins are homodimers of 1164 residues that exhibit 34% and 27%, respectively, of sequence identity with human P-gp, which makes them potential candidates to elaborate a 3D model for P-gp using comparative modeling. However, these two structures could not be directly used as a template at least in their dimeric form. There is indeed considerable support from cysteine disulfide crosslinking studies,[21] EM,[11] and fluorescence energy transfer studies[46] for the two NBDs of P-gp to be in close association. This feature is also well supported by recent X-ray structural characterization of the NBDs of other ABC transporters such as Rad50,[47] MJ0796,[48] and BtuCD.[30] In contrast the two NBDs in *E. coli* MsbA structure are as far as 50 Å. The MsbA dimer structure of *V. cholera* shows an arrangement in which the two NBDs are in close association, seemingly in accordance with experimental data on P-gp. However, a closer look at the structure reveals that the two ATP binding sites are located on the faces opposite to the dimer interface, which appears to us as an unnatural configuration as it is in disagreement with several experimental studies.[11,21,30,46–48]

Though MsbA seemed, in terms of sequence identity, a good template candidate to model the P-gp atomic structure, neither *E. coli* nor *V. cholera* could be used in their dimeric form. In order to circumvent this problem and to generate a model for P-gp in agreement with the largest number of experimental data, we used a combination of computational techniques. The different steps of the modeling procedure are explained below. In a first step, each P-gp half was modeled independently using the structure of MsbA monomers from *E. coli*. P-gp is indeed composed of two homologous halves having 36% and 32 % of sequence

TABLE I. Interresidues C_α-C_α Distances Used in Rigid Body Dynamics

Top left panel:

Group	Res1	Res2	Initial	Min. Restr.	Max Restr.	Final	Delta
TM 4–10	S222	1868	81.4	13	23.5	23.6	0.1
	S222	G872	77.7	13	23.5	25.8	0.3
4–12	L227	S993	71.2	8	15	21.4	6.4
	V231	S993	66.5	8	15	18.4	3.4
	W232	S993	62.7	8	15	15.9	0.9
	A233	S993	62.6	8	10	16.5	6.5
5–10	1306	1868	77	15	23.5	18.1	0
	1306	G872	72.6	15	23.5	12.9	2.1
5–11	1306	T945	81.5	15	23.5	24.1	0.6
5–12	A295	S993	66.4	8	15	18.4	3.4
	1299	S993	69.1	8	10	15.2	5.2
	1306	V982	76.6	15	23.5	17.5	0
	1306	G984	77.1	15	23.5	21.9	0
6–10	P350	V874	68.1	8	15	20.4	5.4
	P350	E875	64.4	8	15	17.5	2.5
	P350	M876	64.1	8	15	19.3	4.3
	L339	1868	72.6	15	23.5	15.4	0
	L339	G872	68.2	15	23.5	15.2	0
	L332	Q856	92.5	13.5	19	24.8	5.8
6–11	P350	G939	64.5	8	15	18.1	3.1
	L339	F942	71.4	19.5	23.5	25.6	2.1
	L339	T945	74.4	14.5	23.5	23.6	0.1
6–12	F343	M986	70.7	8	15	15.9	0.9
	G346	G989	63.1	8	15	16.6	1.6
	P350	S993	65.2	8	15	18.1	3.1
	L339	V982	70.6	8	15	11.1	0
	L339	V982	69.4	13.5	23.5	11.5	2
	L339	A985	67.8	14.5	23.5	14.6	0

Bottom left panel:

Group	Res1	Res2	Initial	Min. Restr.	Max Restr.	Final	Delta
	Y117	G955		8	17.5	16.3	0
	Y117	C956		8	17.5	16.7	0
	Y117	F957		8	17.5	15.5	0
TM 2–11	Y118	G955		8	17.5	13.9	0
	Y118	C956		8	17.5	15.1	0
	Y118	F957		8	17.5	14.3	0
	S119	G955		8	17.5	15.4	0
	S119	C956		8	17.5	16.9	0
	S119	F957		8	17.5	15.4	0

Top right panel:

Group	Res1	Res2	Initial	Min. Restr.	Max Restr.	Final	Delta
	L531	S1071	13.6	8	15	12	0
	L531	S1072	11.9	8	15	10.8	0
	L531	G1073	10.7	8	10	8.5	0
	L531	C1074	13.7	8	10	11	1
	L531	G1075	15.9	8	15	13.7	0
	L531	K1076	18.6	8	15	16.8	0.8
	S532	S1072	10.7	8	15	10.7	0
	S532	G1073	9.8	8	10	9.2	0
	S532	C1074	12.1	8	15	10.9	0
	S532	G1075	15	8	15	14.2	0
	G533	S1072	10.1	8	15	9.7	0
	G533	G1073	10.6	8	15	9.6	0
	G533	C1074	12.8	8	15	11.7	0
NBD–NBD	G534	S1071	13.9	8	15	13.3	0
	G534	S1072	13.6	8	15	12.9	0
	Q535	S1071	16.8	8	15	16.1	1.1
	S429	L1176	13.8	8	15	13	0
	G430	L1176	11.8	8	15	10.3	0
	C431	L1176	14.6	8	10	12.5	2.5
	G432	L1176	16.4	8	15	14.8	0
	S429	S1177	12.2	8	15	12.2	0
	G430	S1177	10.7	8	15	10.1	0
	C431	S1177	13	8	15	12.2	0
	G432	S1177	15.5	8	15	15	0
	S429	G1179	13.8	8	15	13.8	0
	L531	C1074	13.7	8	10	11	1
	C431	L1176	14.6	8	10	12.5	2.5

Bottom right panel:

Group	Res1	Res2	Initial	Min. Restr.	Max Restr.	Final	Delta
	G317	N753		8	17.5	20.8	3.3
	G317	L754		8	17.5	20.6	3.1
	G317	F755		8	17.5	19	1.5
TM 5–8	T318	N753		8	17.5	21.7	4.2
	T318	L754		8	17.5	20.7	3.2
	T318	F755		8	17.5	17.2	0
	T319	N753		8	17.5	18.3	0.8
	T319	L754		8	17.5	17.6	0.1
	T319	F755		8	17.5	14	0

In each panel, the first column indicates the pair of TM helices (or NBDs) involved; the second and third columns give the residue number in each pair; the third column denotes the initial distance value measured in the initial model (before the rigid body dynamics); the fourth and fifth columns indicate the minimal and maximal values respectively of the restraints applied in the dynamics (see the Materials and Methods section); the sixth column shows the distance value in the final model and the seventh column gives the deviation either to the minimum or the maximum distance value in the restraint potentials. All distances are in Angströms (Å).
Top left panel: residues in helices 4, 5, 6, 10, 11, and 12.
Top right panel: residues in the two NBDs.
Bottom panels: residues involved in helices 2, 5, 8, and 11.

identity, respectively, with each MsbA monomer from *E. coli*. Moreover, each MsbA monomer contains six helices as in each half of the P-gp TM domains. The choice of *E. coli* MsbA, despite a better resolution of the *V. cholera* struc-

ture, was mainly guided by the fact that the sequence identity to P-gp is higher for the *E. coli* protein. Notwithstanding the influence of this template on the final model of P-gp will be strongly altered in the following steps which

will transform the initial model by accounting for structural data from P-gp.

In a second step we built an initial model of the P-gp NBD dimer. For this purpose, we resorted to comparative modeling, using two templates: the NBD dimer of *E. coli* BtuCD, the vitamin B_{12} importer, and each NBD monomer of *E. coli* MsbA. The working hypothesis behind this step is that there is considerable support that the NBDs in P-gp form an interface in its resting state, though possibly not a tight one, as shown by cysteine disulfide crosslinking experiments realized in absence of ATP.[21,49] In that respect, BtuCD provides a good template for the relative position and orientation of the NBDs in P-gp. Each MsbA NBD was used as a template to model the internal conformation of each NBD monomer of P-gp.

Each P-gp half, modeled in the first step, was thereafter fitted on the modeled P-gp NBD dimer. The resulting model describes a structure in which the NBDs are in close contact as expected but in which the helices of the two TM domains are as far as 50 Å at their largest separation. This feature, however, is in complete disagreement with the experimental data obtained from the cysteine disulfide cross-linking studies that demonstrate that distance values between the two TM domains should not exceed 25 Å.[19] Moreover in this model some of the residues proposed to be involved in the drug binding were not oriented towards the protein interior.

To solve these discrepancies between the model and the experimental data, molecular dynamics simulations were performed on the model reduced to portions involved in the drug and nucleotide binding, namely the TM helices 4, 5, 6, 10, 11, and 12 and the two NBDs. Each of these portions was defined as a rigid body to keep their internal structure as derived from the comparative modeling stage. Those rigid bodies were allowed to move and reorient subjected to a classical force field and to additional distance-based restraint potentials. These distances were derived from cysteine crosslinking studies in which a single cysteine was introduced in each P-gp half and either an oxydant (Ref. 16, and references therein) or MTS-specific crosslinkers containing 2 to 17 atoms spacer arms[18,19] were used. In the TM domains, 28 double mutants were found to be crosslinked, revealing distances from 8 to 23.5 Å. For the NBDs, 27 crosslinked proteins were observed from which restraints were derived, with distances from 8 to 15 Å (see Methods section for a detailed description of the derivation of the restrained distances and Table I).

This partial model was then completed by adding missing portions using experimental data whenever available. More recent crosslinking data have shown that TM helix 2 is close to TM helix 11 at both intracellular and extracellular ends, with distances value ranging from 8 to 17.5 Å.[27] This observation also holds true for TM helices 5 and 8. To position helix 3, we took into consideration that the extracellular loop between helices 3 and 4 is very short and thus that helix 3 on that side of the cell cannot, therefore, be far from helix 4. The same reasoning was made for helix 9 and 10. These structural data, summarized in Table I, were introduced into a second run of rigid body molecular dynamics simulation to produce a new model. The model obtained in the previous step was defined as a rigid body, and TM helices 2, 5, 8, and 11 formed four additional rigid bodies. Finally the loops connecting the TM helices to the NBDs were added by comparative modeling using as additional templates segments from the initial model of each P-gp half.

The TM1 and TM 7 helices that are not involved in the substrate binding were not modeled because no experimental data were available. Likewise the linker region between the two P-gp halves, which consists of a segment of ~ 60 residues, was not modeled. It has been experimentally shown that its absence does not affect the protein function.[7]

The final model is shown in Figure 2. Its stereochemistry was assessed with Procheck NMR[50] and is consistent with X-ray structures determined at a resolution of 2.0 Å. All the interresidue distances involved in restraints were checked in regard to the experimentally derived data (see Table I for final distance values). The agreement is quite good as the average deviation on all distances is 1.2 Å and the maximum deviation observed is 6.5 Å. The interresidue distances values that deviate most from the restraint values belong to the TM helices. These discrepancies could in part arise from the fact that the restraints were not derived from a single experiment, but from different disulfide crosslinking involving each a particular double mutant. As a result it is possible that all experimental restraints could not be fully satisfied at the same time in one structure. An example of this involves the subsequent residues V231, W232, and A233 (on helix 4) which are experimentally observed to be at a similar distance from residue S993 (on helix 12). All these three residues belong to a helix and consequently can not simultaneously face the P-gp central cavity and S993. This suggests that possible conformational changes involving rotation of the TM helices along their axis may occur as this was shown in P-gp upon ATP hydrolysis.[18]

Visual inspection shows that the model presents a bundle of parallel helices, with a pseudo twofold symmetry axis in the middle of the bundle, parallel to the helices (Fig. 2). The TM domains forms a volume of roughly 65 × 56 × 40 Å, which is in very good agreement with the recent EM structure of P-gp whose resolution is 8 Å,[12] and whose TM domain dimensions are 70 × 60 × 40 Å. Some openings are observed between the helices, notably between TM helices 5 and 8 on one hand and TM helices 2 and 11 on the other hand. They both lead to a large cavity which occupies the center of the helix bundle and is open towards the extracellular side. It is important to note that the openings are not due to the absence of TM helices 1 and 7 in the model. Based on mutagenesis experiences on P-gp[51] and on the crystal structure of MsbA,[29] those two helices are believed to be in the vicinity of TM helices 6 and 12, respectively [see Fig. 2(B)]. The existence of such lateral openings has been observed in EM studies of P-gp.[9] It has been proposed that their role is to allow the P-gp substrates to move from the bilayer inner leaflet into the protein central cavity.[52] The NBDs are in close interaction, and extend on a surface
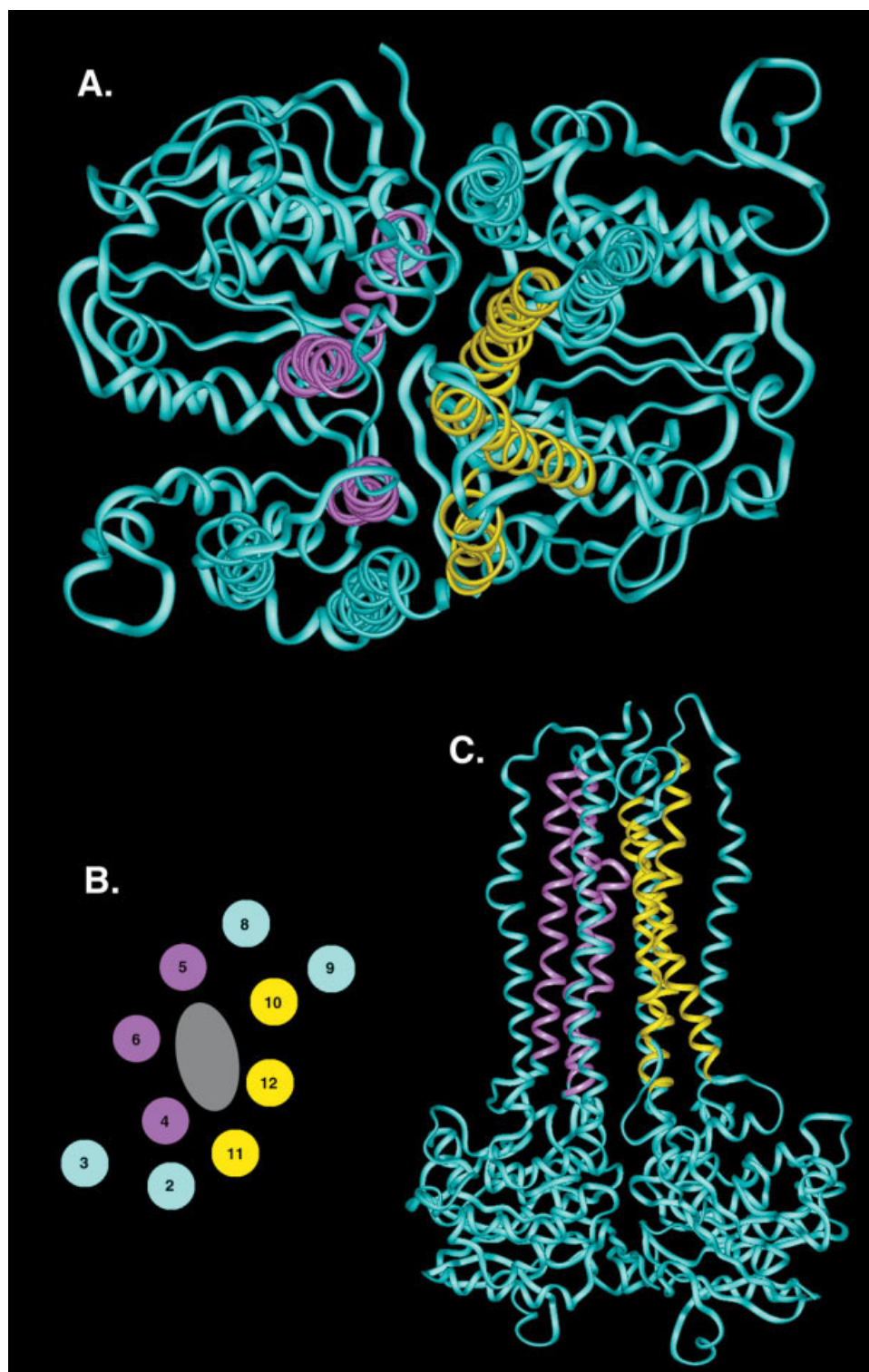
Fig. 2.   Ribbon representation of the 3D model of P-gp. Helices 4, 5, and 6 are colored in pink while helices 10, 11, and 12 are colored in yellow. Those six helices contribute to the cavity wall and are involved in drug binding. (**A**) Top view from the extracellular side. Note the pseudo twofold symmetry axis, with the axis perpendicular to the figure. (**B**) Diagram showing the relative positions of the TM helices in the model. The grey oval in the middle of the helices suggests the position of the drug binding site. (**C**) Longitudinal view across the membrane of the bundle of helices.

TABLE II. List of the Interactions between Atoms of the Docked Ligands (partner 1) and Residues in the P-gp Model (partner 2)

Partner 1		Partner 2	Type of Interaction	Notes
Rhodamine 1	$>N^+ =$	Tyr316 aromatic moiety	Cation-π	In the vicinity of Leu975 and Val982
	—COO$^-$	Ser979 —OH	H-bond	
Rhodamine 2	$>N^+ =$	Tyr953 aromatic moiety	Cation-π	In the vicinity of Ile340, Phe343,
	Ar2	Trp232 aromatic moiety	π-π stacking	Val981 and Val982
	O in the cycle	Trp232 NH	H-bond	
Rhodamine 3	$>N^+ =$	Tyr953 aromatic moiety	Cation-π	In the vicinity of Ile340, Phe343,
	Ar2	Trp232 aromatic moiety	π-π stacking	Val981 and Val982
	O in the cycle	Trp232 NH sidechain	H-bond	
Verapamil 1	Ar2	Phe343 aromatic moiety	π-π stacking	In the vicinity of Leu339 and Ala342
	—O—CH$_3$ on Ar1	Tyr310 —OH	H-bond	
	—O—CH$_3$ on Ar2	Ser228 —OH	H-bond	

See Figure 3 for a representation of the chemical structure of the docked ligands with the numbering of their cycles. The last column specifies the residues experimentally known to be involved in the ligand binding and which are found to interact with the docked structures. For rhodamine numbers 1, 2, and 3 refer to three different positions for the docked molecule.

of roughly 74 × 47 Å, which is in excellent agreement with the 68 × 45 Å measured on the P-gp structure obtained by EM in a lipid environment.[11] The interface between the TM domains and the NBDs in ABC transporters is likely to play a role in the transmission of the conformational change produced by ATP binding and (or) hydrolysis. In our model, this interface is predominantly formed by the Q-loop (residues 475–483 in NBD1 and 1018–1026 in NBD2), a protein region that has been proposed to act as a γ-phosphate sensor prone to change its conformation upon ATP binding and (or) hydrolysis.[53,54] It is interesting to note that the Q-loop in our model is indeed located in the vicinity of the Walker A motif, where ATP binding occurs. This packing is similar to that observed in the BtuCD X-ray structure.[30]

Other P-gp Models

An atomic level structure of P-gp has been modeled by Seigneuret and Garnier-Suillerot.[26] It was determined using comparative modeling using the dimer structure of *E. coli* MsbA as a sole template. As a consequence, the resulting model resembles the structure of the MsbA dimer with a large inner chamber open to the cytoplasmic side. The presence of this chamber, accessible from the lipid bilayer, is supported by an EM study.[10] This is, however, the only point of concordance because the EM structure features a V form, inverted relative to this P-gp model, with a large opening to the extracellular side that is closed at the cytoplasmic face of the membrane. The authors of the model suggested that the model could be a representation of an open structure of P-gp opposed to a closed conformation. However, their modeled structure, with a distance as large as 50 Å between the two NBDs and the cytoplasmic ends of the TM domains, is in total disagreement with the cysteine disulfide crosslinking experiments. It is only upheld by the shape of the dimeric structure of *E. coli* MsbA. One can however not completely exclude the possibility that during the catalytic cycle conformational changes lead to an open conformation as in

the MsbA structure though no structural data on P-gp has backed up this type of structure yet. While this model comprises the full P-gp sequence, it was derived based solely on MsbA structure and therefore includes no structural information from P-gp.

Another 3D atomic model was developed by Stenham and colleagues.[27] In their work, an initial structure of P-gp was generated using the *E. coli* MsbA dimer structure. These authors then applied global translations and rotations on each modeled P-gp half to close the structure. It has indeed been shown by Lee and colleagues[11] that it is only when the two MsbA monomers are rotated to bring their NBDs together that the X-ray structure of MsbA is consistent with the EM projection structure of P-gp. Energy minimization was then performed to optimize the packing of the two TM domains. The resulting model is in relatively good agreement with a number of crosslinking data. However, a few inter-TM domains residue distances were not correctly reproduced by the model and other crosslinking data involving TM residues were not checked against the model. Also no inter-NBD experimental residue distances were considered to validate their structure. Furthermore, each P-gp half structure was modeled from each MsbA monomer without any alteration. We showed that in such a model some residues involved in substrate binding are located on helix faces opposite to the drug binding cavity suggesting that MsbA monomer cannot be used as a rigid structure to model each P-gp half.

Pajeva and colleagues[28] presented in a recent work a partial model of the TM domain of P-gp, describing the protein in the bound-nucleotide state. Each helix was first independently built by modeling. All helices were then subjected to an energy minimization including restraints between some of the TM residues involved in crosslinking. Though no real docking was performed, this model was used to identify potential binding sites for two different ligands including rhodamine. This model was elaborated based only on structural information derived from P-gp. Furthermore, it includes only a restricted number of TM
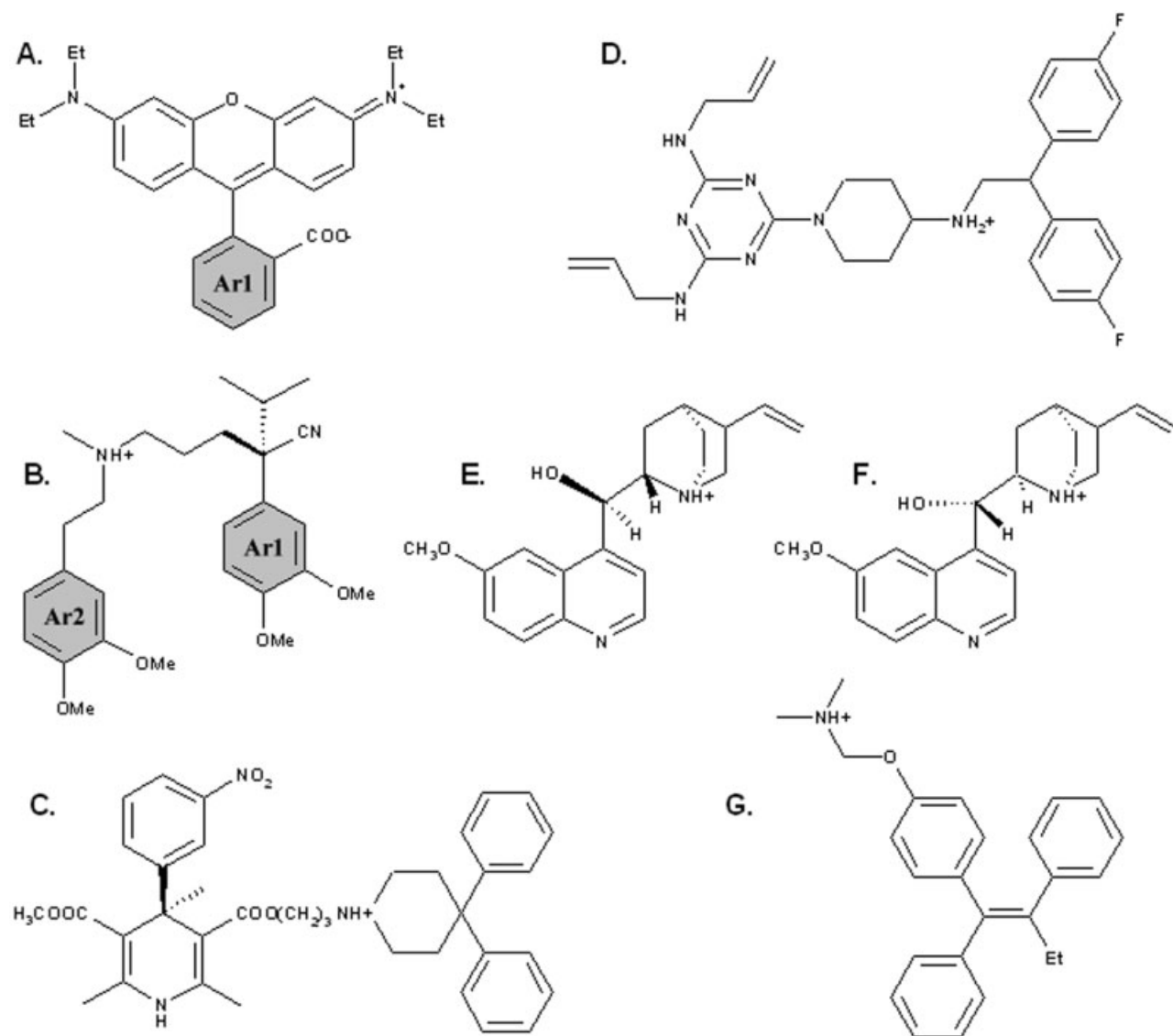
Fig. 3. Chemical structures of the different ligands. (**A**) Rhodamine; (**B**) verapamil; (**C**) dexniguldipine; (**D**) S9788; (**E**) quinine; (**F**) quinidine; and (**G**) tamoxifen. The Ar1 and Ar2 in rhodamine and verapamil describe specific aromatic moieties involved in interactions with P-gp model upon docking (see Table II).

helices, those directly involved in drug binding, and lacks the NBDs.

Ligand Docking into P-gp Model

In order to further assess the quality of the model, we performed the docking of a number of P-gp ligands. The scope is double. First, to verify whether not only the cavity, but also the lateral holes, are large enough to accommodate P-gp ligands, we performed the docking of two known P-gp ligands: verapamil and rhodamine (Fig. 3). Protein residues in contact with these two compounds have been identified.[17,22] Second, we selected six inhibitors for which K_i values have been reported in a comparative study.[42] Docking was performed for dexniguldipine, S9788, quinidine, verapamil, tamoxifen, and quinine (Fig. 3). Only first and second generation inhibitors of P-gp have been se-

lected, as third generation inhibitors are not competitive inhibitors, that is, their binding doesn't occur in the cavities of the TM domains.

For verapamil and rhodamine, 25 independent docking runs were performed in a zone surrounding the lateral opening between helices 5 and 8 on one hand, and in the central cavity on the other hand.

The position of the mass center of the molecules docked in the central cavity reveals that each ligand can occupy different positions. For verapamil, the positions of the mass centers are spread throughout the whole cavity while for rhodamine three different clusters are found, which contain 18 of the 25 mass centers. The geometry of interaction of the docked ligands with P-gp was examined in minute detail for five structures of each ligand selected on the basis of their best affinity.
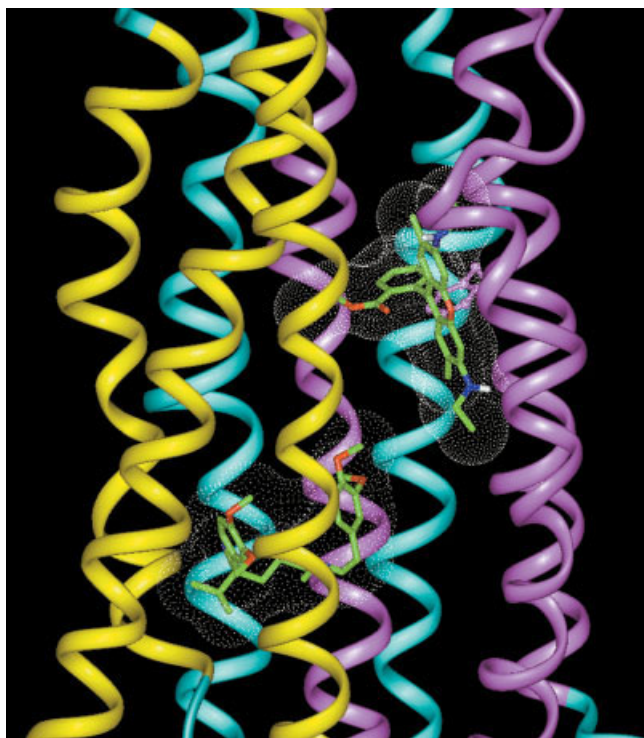
Fig. 4. Ribbon representation of the P-gp model: longitudinal view across the membrane. Two different ligands could be accommodated in the central cavity (rhodamine in the upper right; verapamil in bottom left). Helices 4, 5, and 6 are colored in pink; helices 10, 11, and 12 in yellow, and the other helices in cyan. The docked ligands are depicted as sticks and colored following their atom type (green for carbon; red for oxygen; blue for nitrogen; and white for hydrogen). Their molecular surface is also shown.
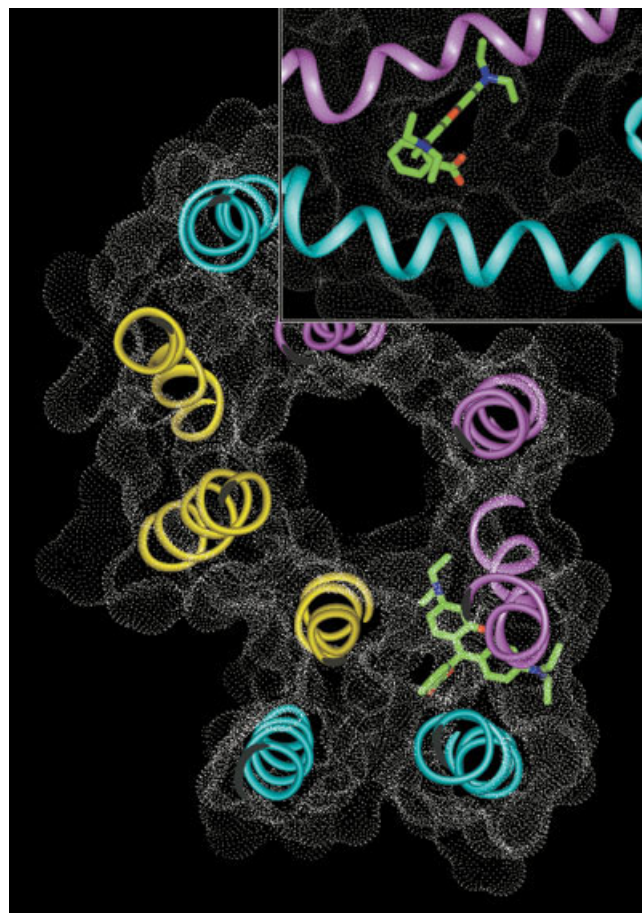

Fig. 5. Top view from the extracellular side of a cross-section of the P-gp model depicted as a ribbon and by its molecular surface. The central cavity prone to harbor ligands is located in the middle of the protein. A molecule of rhodamine has been docked between helices 5 and 8 in a lateral opening leading to the central cavity. Helices 4, 5, and 6 are colored in pink; helices 10, 11, and 12 in yellow; and the other helices in cyan. The docked rhodamine molecule is colored following its atom type (green for carbon; red for oxygen; and blue for nitrogen). Inset: Lateral view, illustrating the lateral opening between helices 5 and 8 and a docked rhodamine molecule. Note that the aromatic cycles and one of the amines are in the opening, while the other amine group lies on external surface of the protein.

Certain residues of P-gp involved in rhodamine binding have been identified by cysteine scanning mutagenesis.[22] They are located on TM helices 6, 9, 11, and 12. One of the five docked structures is located close to Leu975 and Val982 in TM12. Two other rhodamine molecules are close to residues Ile340, Phe343 (TM6), Val981, and Val982 (TM12). All these residues have been experimentally found to be involved in the binding of the drug. Table II describes the interactions between these three structures and P-gp. Each forms one H-bond and at least one π–π or one cation–π interaction. The residues involved in the verapamil binding have also been identified by cysteine scanning mutagenesis.[17] They pertain to helices 4, 6, 10, 11, and 12. The inspection of the positions of the five structures docked into P-gp reveals that only one of them is close to binding site residues Leu339 and Ala342. Interactions with the P-gp model are reported in Table II.

The drug binding site cavity in the model shows that one rhodamine molecule cannot bind at the same time to all residues experimentally proposed to be involved in binding: the distances between some of them are just too large. This also holds for verapamil. Several studies have presented evidence for the existence of multiple drug interaction sites. Dey and colleagues,[55] for example, reported that iodoarylazidoprazosin has two nonidentical drug interaction sites in P-gp. In another P-gp model, Pajeva and colleagues[28] discussed the existence of two distinct sites of

binding for rhodamine, one in the vicinity of TM6 and the other in the vicinity of TM12. Furthermore, it has been shown that the binding cavity is large enough to accommodate two molecules at the same time. By resorting on drug binding measurements, Pascaud and colleagues[56] showed that while verapamil inhibits vinblastine binding, it has no effect on nicardipine binding, meaning that those two ligands have distinct specific sites of binding. By cysteine scanning experiments, Loo and colleagues[23] revealed that upon binding of a derivated rhodamine binding of verapamil is still possible. The P-gp model we present here does allow positioning these two ligands in the central cavity of our model (Fig. 4). Among the five docked verapamil structures, three are compatible with this double-ligand binding and all of them form at least two H-bonds with P-gp.

Rhodamine (see Fig. 5) and verapamil were successfully docked into the lateral opening between helices 5 and 8. More

TABLE III. Inhibition Constants Measured Experimentally[42] and Calculated by Docking (Average over the 25 Runs)

K_i/M	Dexniguldipine	S9788	Quinidine	Verapamil	Tamoxifen	Quinine
Experiment	$3.7\,10^{-8}$	$2.5\,10^{-7}$	$2.7\,10^{-7}$	$6.0\,10^{-7}$	$8.0\,10^{-7}$	$1.9\,10^{-6}$
Docking	$1.5\,10^{-6}$	$8.4\,10^{-6}$	$1.6\,10^{-5}$	$3.6\,10^{-5}$	$4.1\,10^{-5}$	$4.0\,10^{-5}$
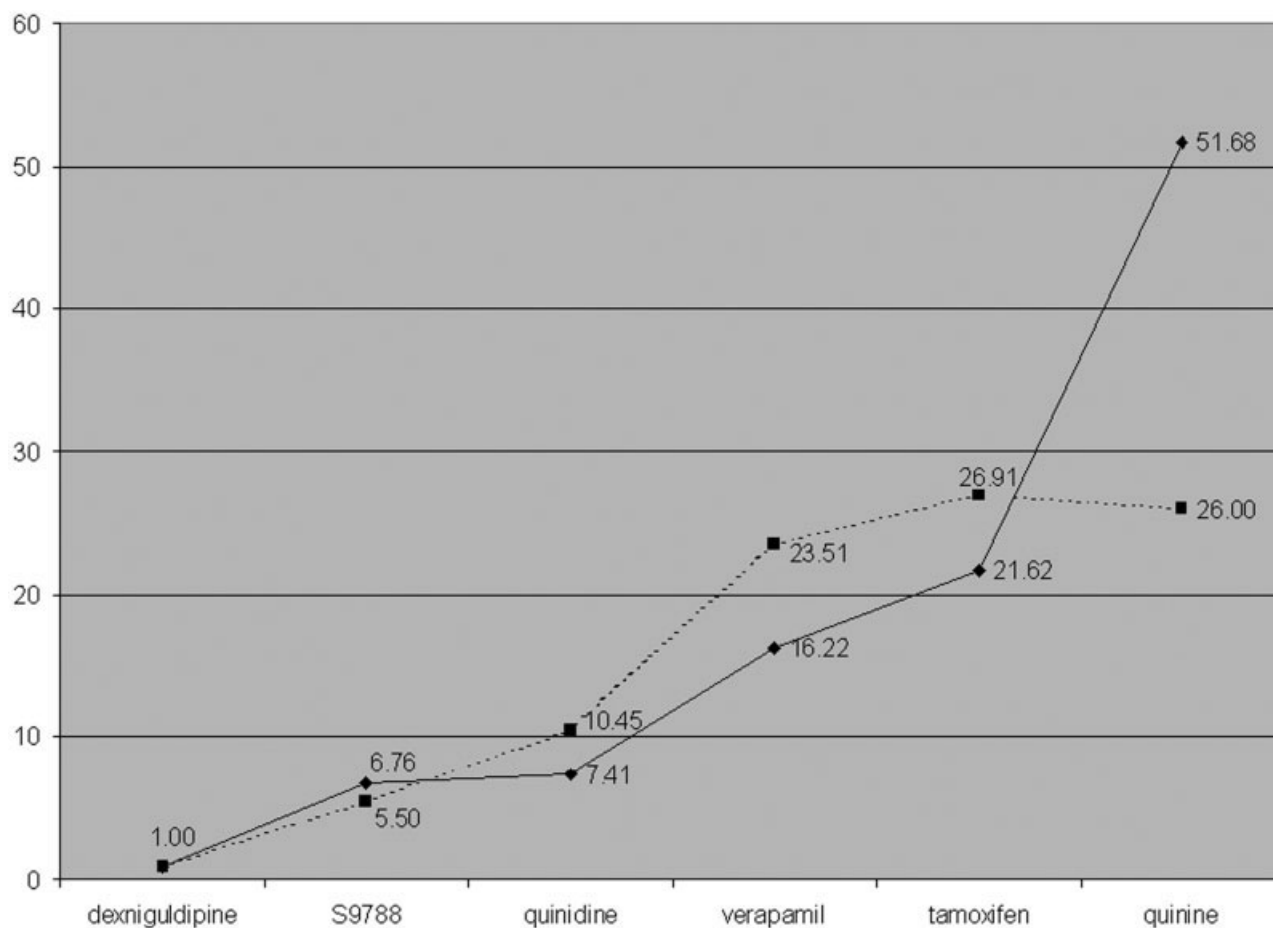
Fig. 6. Comparison of experimental and calculated affinities for known P-gp inhibitors, expressed as relative K_i. Experimental data values are shown as a solid line and diamonds; calculated docking values are shown as a dashed line and squares.

precisely for rhodamine, the two aromatic cycles (Fig. 5) are engaged in the hole, while one of its amines lies on the external surface of the protein. The capacity of the 3D model to feature a possible passage of the ligand from the bilayer into the central cavity is another important feature, because it has been proposed that, after the transfer from the cytoplasm to the inner bilayer, the drug diffuses through a lateral opening from the bilayer to the binding site.[52]

For dexniguldipine, S9788, quinidine, verapamil, tamoxifen, and quinine, 25 independent docking runs were performed in the central cavity for each inhibitor. The average affinity for P-gp of each docked compound, expressed as a K_i, is compared to the experimental value in Table III. All calculated K_i values underestimate the inhibition. This is not surprising, as such a systematic error on the evaluation of affinity often occurs in docking experiments. A calibration of

the evaluation function on a set of known ligands can circumvent this. To do so we expressed the calculated K_i values relative to dexniguldipine, the strongest inhibitor. The results are shown in Figure 6. A clear correlation between experimental and calculated values is obtained. For example, tamoxifen is predicted to be 26.91 less active than dexniguldipine, to be compared with an experimental value of 21.62. The only exception is quinine whose predicted relative affinity is underestimated. This result is somewhat surprising as the affinity of its diastereoisomer, quinidine, is better predicted.

One can argue that performing docking on this particular 3D model is a bit perilous. However, our concern was first to verify whether the model is prone to accommodate known P-gp ligands in the lateral openings. Second, the docking of different ligands into the central cavity of the

protein was found to agree pretty well with experimental data. As such these docking results add credit to the validity of the model.

CONCLUSION

Unlike other models, the model described here was generated using a combination of various *in silico* methods including all possible structural information on both the TM domains and the NBDs derived from crosslinking studies on P-gp. This atomic level model of the protein in absence of ATP is quite complete (with 10 helices and both NBDs) and coherent because experimental data for P-gp related to this structure were carefully selected. The modeled structure is in good agreement with the structure of P-gp obtained by EM in a lipid environment. Like the EM-derived structure, our model features a closed conformation with the two NBDs in interaction. Its size and shape are also in good accordance with these EM data. In addition to these characteristics, the 3D model presented here shows the existence of an internal cavity prone to accommodate different P-gp ligands. The mode of association observed for the docked ligands favors the existence of multiple binding sites in the protein, a feature supported by several experimental studies. Predicted and experimental affinities correlate well. For each of the ligands, one or more positions were found to involve interactions with residues identified by cysteine-scanning experiments as binding these drugs. In particular, several types of interactions with these residues, such as H-bonds, $\pi-\pi$ or cation$-\pi$ interactions, were recognized and are consistent with a pharmacophore model elaborated from P-gp ligands. Furthermore, the central cavity is connected to the outside by a lateral opening which is large enough to allow the transit of the three ligands studied here. This finding corroborates the commonly admitted mechanism of substrate uptake from the lipid bilayer.

This model may, therefore, constitute a useful starting point for the understanding of the complete structural picture of P-gp along its catalytic mechanism.

REFERENCES

1. Higgins CF. ABC transporters: physiology, structure and mechanism — an overview. Res Microbiol 2001;152:205–210.
2. Lin JH, Yamazaki M. Role of P-glycoprotein in pharmacokinetics: clinical implications. Clin Pharmacokinet 2003;42:59–98.
3. Leonard GD, Fojo T, Bates SE. The role of ABC transporters in clinical practice. Oncologist 2003;8:411–424.
4. Van Bambeke F, Balzi E, Tulkens PM. Antibiotic efflux pumps (Commentary). Biochem Pharmacol 2000;15:457–470.
5. Higgins CF, Linton KJ. The ATP switch model for ABC transporters. Nat Struct Mol Biol 2004;11:918–926.
6. Ambudkar SV, Dey S, Hrycyna CA, Ramachandra M, Pastan I, Gottesman MM. Biochemical, cellular, and pharmacological aspects of the multidrug transporter. Annu Rev Pharmacol Toxicol 1999;39:361–398.
7. Hrycyna CA, Airan LE, Germann UA, Ambudkar SV, Pastan I, Gottesman MM. Structural flexibility of the linker region of human P-glycoprotein permits ATP hydrolysis and drug transport. Biochemistry 1998;37:13660–13673.
8. Vigano C, Julien M, Carrier I, Gros P, Ruysschaert JM. Structural and functional asymmetry of the nucleotide-binding domains of P-glycoprotein investigated by attenuated total reflection Fourier transform infrared spectroscopy. J Biol Chem 2002;277:5008–5016.
9. Rosenberg MF, Velarde G, Ford RC, Martin C, Berridge G, Kerr ID, Callaghan R, Schmidlin A, Wooding C, Linton KJ, Higgins CF. Repacking of the transmembrane domains of P-glycoprotein during the transport ATPase cycle. EMBO J 2001;20:5615–5625.
10. Rosenberg MF, Callaghan R, Ford RC, Higgins CF. Structure of the multidrug resistance P-glycoprotein to 2.5 nm resolution determined by electron microscopy and image analysis. J Biol Chem 1997;272:10685–10694.
11. Lee JY, Urbatsch IL, Senior AE, Wilkens S. Projection structure of P-glycoprotein by electron microscopy. Evidence for a closed conformation of the nucleotide binding domains. J Biol Chem 2002;277:40125–40131.
12. Rosenberg MF, Callaghan R, Modok S, Higgins CF, Ford RC. Three-dimensional structure of P-glycoprotein. J Biol Chem 2005; 280:2857–2862.
13. Ruth A, Stein WD, Rose E, Roninson IB. Coordinate changes in drug resistance and drug-induced conformational transitions in altered-function mutants of the multidrug transporter P-glycoprotein. Biochemistry 2001;40:4332–4339.
14. Greenberger LM. Major photoaffinity drug labeling sites for iodoaryl azidoprazosin in P-glycoprotein are within, or immediately C-terminal to, transmembrane domains 6 and 12. J Biol Chem 1993;268:11417–11425.
15. Loo TW, Clarke DM. Drug-stimulated ATPase activity of human P-glycoprotein requires movement between transmembrane segments 6 and 12. J Biol Chem 1997;272:20986–20989.
16. Loo TW, Clarke DM. The packing of the transmembrane segments of human multidrug resistance P-glycoprotein is revealed by disulfide cross-linking analysis. J Biol Chem 2000;275:5253–5256.
17. Loo TW, Clarke DM. Defining the drug-binding site in the human multidrug resistance P-glycoprotein using a methanethiosulfonate analog of verapamil, MTS-verapamil. J Biol Chem 2001;276: 14972–14979.
18. Loo TW, Clarke DM. Cross-linking of human multidrug resistance P-glycoprotein by the substrate, tris-(2-maleimidoethyl)amine, is altered by ATP hydrolysis. Evidence for rotation of a transmembrane helix. J Biol Chem 2001;276:31800–31805.
19. Loo TW, Clarke DM. Determining the dimensions of the drug-binding domain of human P-glycoprotein using thiol cross-linking compounds as molecular rulers. J Biol Chem 2001;276:36877–36880.
20. Loo TW, Clarke DM. Vanadate trapping of nucleotide at the ATP-binding sites of human multidrug resistance P-glycoprotein exposes different residues to the drug-binding site. Proc Natl Acad Sci U S A 2002;99:3511–3516.
21. Loo TW, Bartlett MC, Clarke DM. The LSGGQ motif in each nucleotide-binding domain of human P-glycoprotein is adjacent to the opposing walker A sequence. J Biol Chem 2002;277:41303–41306.
22. Loo TW, Clarke DM. Location of the rhodamine-binding site in the human multidrug resistance P-glycoprotein. J Biol Chem 2002;277: 44332–44338.
23. Loo TW, Bartlett MC, Clarke DM. Methanethiosulfonate derivatives of rhodamine and verapamil activate human P-glycoprotein at different sites. J Biol Chem 2003;278:50136–50141.
24. Loo TW, Bartlett MC, Clarke DM. Val[133] and Cys[137] in transmembrane segment 2 are close to Arg[935] and Gly[939] in transmembrane segment 11 of human P-glycoprotein. J Biol Chem 2004;279:18232–18238.
25. Rothnie A, Storm J, Campbell J, Linton KJ, Kerr ID. The topography of transmembrane segment six is altered during the catalytic cycle of P-glycoprotein. J Biol Chem 2004;279:34913–34921.
26. Seigneuret M, Garnier-Suillerot A. A structural model for the open conformation of the mdr1 P-glycoprotein based on the MsbA crystal structure. J Biol Chem 2003;278:30115–30124.
27. Stenham DR, Campbell JD, Sansom MS, Higgins CF, Kerr ID, Linton KJ. An atomic detail model for the human ATP binding cassette transporter P-glycoprotein derived from disulfide cross-linking and homology modeling. FASEB J 2003;17:2287–2289.
28. Pajeva, IK, Globisch C, Wiese M. Structure-function relationships of multidrug resistance P-glycoprotein. J Med Chem 2004;47:2523–2533.
29. Chang G, Roth CB. Structure of MsbA from *E. coli*: a homolog of the multidrug resistance ATP binding cassette (ABC) transporters. Science 2001;293:1793–1800.
30. Locher KP, Lee AT, Rees DC. The *E. coli* BtuCD structure: a framework for ABC transporter architecture and mechanism. Science 2002;296:1091–1098.

31. Pajeva IK, Wiese M. Pharmacophore model of drugs involved in P-glycoprotein multidrug resistance: explanation of structural variety (hypothesis). J Med Chem 2002;45:5671–5686.

32. Thompson JD, Higgins DG, Gibson TJ. CLUSTAL W: improving the sensitivity of progressive multiple sequence alignment through sequence weighting, position-specific gap penalties and weight matrix choice. Nucleic Acids Res 1994;22:4673–4680.

33. Holm L, Sander C. Database algorithm for generating protein backbone and side-chain co-ordinates from a C alpha trace application to model building and detection of co-ordinate errors. J Mol Biol 1991;218:183–194.

34. Altschul SF, Gish W, Miller W, Myers EW, Lipman DJ. Basic local alignment search tool. J Mol Biol 1990;215:403–410.

35. Sali A, Blundell TL. Comparative protein modelling by satisfaction of spatial restraints. J Mol Biol 1993;234:779–815.

36. Chun HM, Padilla CE, Chin DN, Watanabe M, Karlov VI, Alper HE, Soosaar K, Blair KB, Becker OM, Caves LSD, Nagle R, Haney DN, Farmer BL. MBO(N)D: a multibody method for long-time molecular dynamics simulations. J Comput Chem 2000;21:159–184.

37. Brooks BR, Bruccoleri RE, Olafsson D, States D, Swaminathan S, Karplus M. CHARMM: a program for macromolecular energy minimization and dynamics calculations. J Comput Chem 1983;4:187–217.

38. MacKerell AD Jr, Bashford D, Bellott M, Dunbrack Jr RL, Evanseck JD, Field MJ, Fischer S, Gao J, Guo H, Ha S, Joseph-McCarthy D, Kuchnir L, Kuczera K, Lau FTK, Mattos C, Michnick S, Ngo T, Nguyen DT, Prodhom B, Reiher III WE, Roux B, Schlenkrich M, Smith JC, Stote R, Straub J, Watanabe M, Wiorkiewicz-Kuczera J, Yin D, Karplus M. All-atom empirical potential for molecular modeling and dynamics studies of proteins. J Phys Chem B 1998;102:3586–3616

39. Sadowski J, Gasteiger J. From atoms and bonds to three-dimensional atomic coordinates: automatic model builders. Chem Rev 1993;93:2567–2581.

40. Canutescu AA, Shelenkov AA, Dunbrack RL Jr. A graph-theory algorithm for rapid protein side-chain prediction. Protein Sci 2003;12:2001–2014.

41. ChemSilico LLC. http://chemsilico.com/

42. Ferry DR, Traunecker H, Kerr DJ. Clinical trials of P-glycoprotein reversals in solid tumours. Eur J Cancer 1996;32A:1070–1081.

43. Stewart JJ. MOPAC: a semiempirical molecular orbital program. J Comput Aided Mol Des 1990;4:1–105

44. Morris GM, Goodsell DS, Halliday RS, Huey R, Hart WE, Belew RK, Olson AJ. Automated docking using a Lamarckian genetic algorithm and empirical binding free energy function. J Comput Chem 1998;19:1639–1662.

45. Chang G. Structure of MsbA from *Vibrio cholera*: a multidrug resistance ABC transporter homolog in a closed conformation. J Mol Biol 2003;330:419–430.

46. Qu Q, Sharom FJ. FRET analysis indicates that the two ATPase active sites of the P-glycoprotein multidrug transporter are closely associated. Biochemistry 2001;40:1413–1422.

47. Hopfner KP, Karcher A, Shin DS, Craig L, Arthur LM, Carney JP, Tainer JA. Structural biology of Rad50 ATPase: ATP-driven conformational control in DNA double-strand break repair and the ABC-ATPase superfamily. Cell 2000;101:789–800.

48. Smith PC, Karpowich N, Millen L, Moody JE, Rosen J, Thomas PJ, Hunt, JF. ATP binding to the motor domain from an ABC transporter drives formation of a nucleotide sandwich dimer. Mol Cell 2002;10:139–149.

49. Urbatsch IL, Gimi K, Wilke-Mounts S, Lerner-Marmarosh N, Rousseau ME, Gros P, Senior AE. Cysteines 431 and 1074 are responsible for inhibitory disulfide cross-linking between the two nucleotide-binding sites in human P-glycoprotein. J Biol Chem 2001;276:26980–26987.

50. Laskowski RA, MacArthur MW, Moss DS, Thornton JM. PRO-CHECK: a program to check the stereochemical quality of protein structures. J Appl Cryst 1993;26:283–291.

51. Loo TW, Clarke DM. Quality control by proteases in the endoplasmic reticulum. Removal of a protease-sensitive site enhances expression of human P-glycoprotein. J Biol Chem 1998;273:32373–32376.

52. Shapiro AB, Corder AB, Ling V. P-glycoprotein-mediated Hoechst 33342 transport out of the lipid bilayer. Eur J Biochem 1997;250:115–121.

53. Yuan YR, Blecker S, Martsinkevich O, Millen L, Thomas PJ, Hunt JF. The crystal structure of the MJ0796 ATP-binding cassette. Implications for the structural consequences of ATP hydrolysis in the active site of an ABC transporter. J Biol Chem 2001;276:32313–32321.

54. Jones PM, George AM. Mechanism of ABC transporters: a molecular dynamics simulation of a well characterized nucleotide-binding subunit. Proc Natl Acad Sci U S A 2002;99:12639–12644.

55. Dey S, Ramachandra M, Pastan I, Gottesman MM, Ambudkar SV Evidence for two nonidentical drug-interaction sites in the human P-glycoprotein. Proc Natl Acad Sci U S A 1997;94:10594–10599.

56. Pascaud C, Garrigos M, Orlowski S. Multidrug resistance transporter P-glycoprotein has distinct but interacting binding sites for cytotoxic drugs and reversing agents. Biochem J 1998;333:351–358.